X-ray absorption in matter

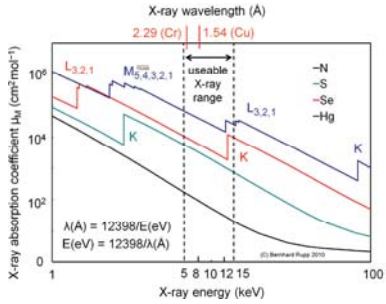

Figure 6-29 X-ray absorption of selected elements. Absorption curves for this figure were calculated using the program FPRIME[17] from relativistic photoelectric cross sections.[18] Note the sharp increase in absorption at specific energies for each element. These absorption edges are labeled (K, L_i and M_i) according to the atomic core level transitions involved (Figure 6-30).

1) Low energy X-rays are more absorbed than high energy
2) Heavier elements absorb stronger than light ones
3) Jumps or edges exist in absorption spectrum

What happens at the absorption edge?

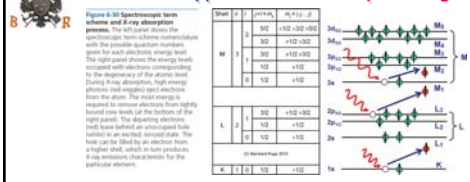

Figure 6-30 Spectroscopic term scheme and X-ray absorption process. The left panel shows the spectroscopic term scheme nomenclature with the possible quantum numbers given for each electronic energy level. The right panel shows the energy levels occupied with electrons corresponding to the degeneracy of the atomic level. During X-ray absorption, high energy photons (red wiggles) eject electrons from the atom. The most energy is required to remove electrons from tightly bound core levels (at the bottom of the right panel). The departing electrons (red) leave behind an unoccupied hole (white) in an excited, ionized state. The hole can be filled by an electron from a higher shell, which in turn produces X-ray emissions characteristic for the particular element.

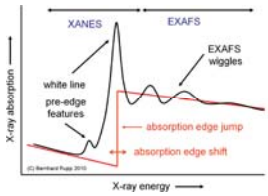

Figure 6-31 The fine structure of an X-ray absorption edge. The figure shows the fine structure of an experimental absorption edge overlaying the theoretically computed edge jump (red step-curve). The features are discussed in detail in the text.

$$f_{(S,\lambda)} = f^{0}_{(S)} + f^{'}_{(\lambda)} + i \cdot f^{''}_{(\lambda)}$$

The atomic scattering factor becomes wavelength dependent and complex

Wavelength dependence and complex component f"

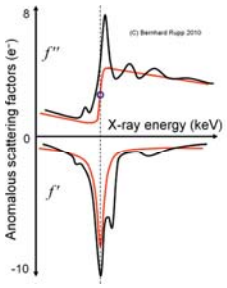

Figure 6-32 Derivation of f' from the normalized X-ray edge scan. The f'' curve is derived by Kramers–Kronig transform of the normalized X-ray edge scan. The red graph depicts the situation ignoring any X-ray edge fine structure, emphasizing that the negative peak of the f' function coincides with the steepest slope at the inflection point (blue circle) of the edge step in the f'' scan.

$$f^{'}_{(\lambda)} = \frac{2}{\pi}\int_{0}^{\infty} E^{'} \cdot \frac{f^{''}_{(E^{'})}}{(E^{2} - E^{'2})} \partial E^{'}$$

The f' component can be directly obtained from edge scan (f") by Kramers-Kronig transform. But what does the i·f" imply for structure factor?

The f" component causes anomalous differences between centrosymmetrically related wedges of a data set

Figure 6-34 Breakdown of Friedel's law through anomalous scattering contributions. The vector $\mathbf{F}_P$ represents the partial sum of all of the non-anomalous atom contributions, and the remaining vectors are the contributions from the anomalously scattering atom, $\mathbf{F}_A$. The real and imaginary components of $\mathbf{F}_A$ are indicated in green ($\mathbf{F}+\mathbf{f}'$) and magenta ($\mathbf{f}''$), respectively. When the indices *hkl* are inverted to –*h*–*k*–*l* as indicated by the (') superscripts, normal scattering contributions are mirrored across the real axis, while the anomalous component becomes mirrored in relation to the imaginary axis. The result is that in the presence of anomalous scattering contributions, Friedel's law breaks down and the structure factor amplitude, and thus the intensity of Bijvoet mates (*F*ʰ and *F*⁻ʰ), becomes different.

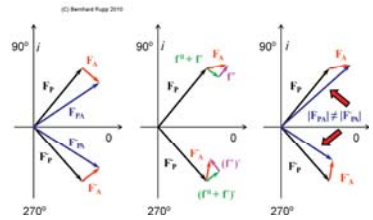

Breaking the centrosymmetry of the diffraction pattern is the basis of powerful and ubiquitous anomalous phasing techniques. The anomalous difference data form the basis for substructure solution.

$$I_{h} \approx F_{h}^{2} = (A_{h} + iB_{h})(A_{h} - iB_{h}) = A_{h}^{2} + B_{h}^{2}$$
$$I_{-h} \approx F_{-h}^{2} = (A_{h} - iB_{h})(A_{h} + iB_{h}) = A_{h}^{2} + B_{h}^{2}$$

X-ray absorption edge energies

E	z	K(eV)	K(Å)	L_1(eV)	L_1(Å)	L_2(eV)	L_2(Å)	L_3(eV)	L_3(Å)	M_5(eV)	M_5(Å)
C	6	283.8	43.6844	–							
N	7	401.6	30.8706	–							
O	8	532.0	23.3038	–							
S	16	2472.0	5.01523	229.2							
Ca	20	4038.1	3.07017	437.8							
Mn	25	6539.0	1.89595	769.0							
Fe	26	7112.0	1.74320	846.1							
Co	27	7708.9	1.60822	925.6							
Ni	28	8332.8	1.48781	1008.1							
Cu	29	8978.9	1.38075	1096.1							
Zn	30	9658.6	1.28359	1193.6							
Se	34	12657.8	0.97945	1652.9							
Br	35	13473.7	0.92014	1782.0							
Kr	36	14325.6	0.86542	1921.0							
Pd	46	24350.5	0.50914	3604.3							
Ag	47	25514.0	0.48592	3805.8	3.25756	3523.7	3.51836	3351.1	3.6996	719.0	17.243
Cd	48	26711.2	0.46414	4018.0	3.08552	3727.0	3.32644	3537.5	3.5046	772.0	16.059
I	53	33169.4	0.37377	5188.1	2.38963	4852.1	2.55511	4557.1	2.7205	1072.0	11.565
Xe	54	34561.4	0.35871	5452.8	2.27343	5103.7	2.42915	4782.2	2.5925	1148.7	10.793
Ba	63	48519.0	0.25552	8052.0	1.53970	7617.1	1.62741	6976.9	1.7770	1800.0	6.8876
Ir	77	76111.0	0.16289	13419.5	0.92392	12824.1	0.96675	11215.2	1.1054	3174.0	3.9060
Pt	78	78394.8	0.15814	13879.9	0.89321	13272.6	0.93408	11563.7	1.0721	3296.0	3.7614
Au	79	80724.9	0.15358	14352.8	0.86378	13733.6	0.90272	11918.7	1.0402	3425.0	3.6197
Hg	80	83102.3	0.14919	14839.3	0.83546	14208.7	0.87254	12283.9	1.0093	3562.0	3.4805
Pb	82	88004.5	0.14088	15860.8	0.78165	15200.8	0.81563	13035.2	0.9511	3851.0	3.2193
U	92	115606.1	0.10724	21757.4	0.56981	20847.6	0.59184	17166.3	0.7222	5548.0	2.2346

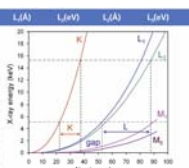

Figure 6-35 Absorption edges in the range useful for anomalous diffraction data collection. Most elements, with the exception of a gap approximately extending over the elements of the 5th period, have K edges in the range of 0.9 Å to 1.5 Å, ideally suitable for most synchrotrons for anomalous MAD diffraction data collection at an absorption edge. Note, however, that any energy above the absorption edge of an element will provide anomalous differences, which allows SAD or SIRAS phasing.

Table 6-4 X-ray absorption edge energies for selected elements. The theoretical atomic absorption edge energies in eV and Å are listed for common elements used in anomalous phasing. The light elements (C, N, O) provide no appreciable anomalous contributions, but beginning with S, a usable anomalous signal can be obtained. Highlighted boxes emphasize elements that can be used for edge-specific, complete MAD experiments in the 5–15 keV window accessible by most synchrotron X-ray sources.

X-ray absorption edge energies and MAD

MAD: multiple anomalous diffraction phasing: uses both anomalous and dispersive differences

Table 6-5 Computed anomalous structure factors for a Se-Met labeled protein. A representative sample of structure factor amplitudes and phases are grouped in centrosymmetrically related pairs. The shading color indicates their phase properties: centric reflections with real structure factors (yellow), general centric reflections (magenta), Friedel pairs with no phase restrictions (orange) or anomalous Bijvoet pairs (white and green). Dispersive differences between the remote and peak wavelength are present for all reflections, while anomalous differences between Friedel pairs exist only for non-centric reflections with unrestricted phases. The anomalous differences are on the order of a few percent of the structure factor amplitude.

	no signal	below edge	maximum f"
Energy eV	–	12458	12658
Wavelength Å	–	0.99518	0.97645
f' (Se)	0.0	-3.6	-5.2
f" (Se)	0.0	0.5	3.8

h	k	l	F(h)(Å)	φ(h)(Å)	F(h)(Å)	F(h)(Å)	centric	dF(h)(Å)	(sin θ/λ)²
2	0	0	82.4	180.0	79.0	77.7	1	37.7	0.000176
-2	0	0	82.4	180.0	79.0	77.7	1	37.7	0.000176
2	0	1	112.2	270.0	113.0	113.5	1	22.8	0.000462
-2	0	-1	112.2	90.0	113.0	113.5	1	22.8	0.000462
2	1	0	116.5	0.0	116.6	117.9	1	19.4	0.000666
-2	-1	0	116.5	0.0	116.6	117.9	1	19.4	0.000666
2	0	1	129.3	270.0	126.8	125.7	1	18.9	0.000702
-2	0	-1	129.3	90.0	126.8	125.7	1	18.9	0.000702
4	0	0	197.0	180.0	198.9	200.0	1	18.9	0.000704
-4	0	0	197.0	180.0	198.9	[illegible]	1	18.9	0.000704
1	1	1	115.2	323.9	113.9	116.3	0	17.3	0.000840
-1	-1	-1	115.2	36.2	112.8	109.2	0	17.3	0.000840
2	1	1	34.4	354.2	35.4	[illegible]	0	16.0	0.000972
-2	-1	-1	34.4	5.9	34.6	33.9	0	16.0	0.000972
4	0	-1	49.8	90.0	50.3	51.4	1	15.7	0.001024
-4	0	-1	49.8	270.0	50.3	51.4	1	15.7	0.001024
3	1	1	72.7	249.3	75.8	77.6	0	14.5	0.001192
-3	-1	-1	72.7	110.7	75.8	75.8	0	14.5	0.001192
1	1	2	69.7	118.7	69.9	69.4	0	11.9	0.001757
-1	-1	-2	69.7	241.3	69.7	70.4	0	11.9	0.001757
2	1	2	45.4	252.1	45.5	44.2	0	11.5	0.001889
-2	-1	-2	45.4	107.9	46.1	46.2	0	11.5	0.001889
1	2	1	59.0	354.6	59.0	61.2	0	10.4	0.002311
-1	-2	-1	59.0	3.5	59.3	58.4	0	10.4	0.002311
4	1	1	104.7	305.0	105.9	108.9	0	10.3	0.002379
-4	-1	-1	104.7	55.0	105.1	105.4	0	10.3	0.002379
1	1	3	111.5	7.4	111.0	108.7	0	8.7	0.003285
-1	-1	-3	111.5	352.6	111.7	114.3	0	8.7	0.003285
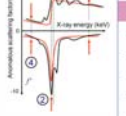
Figure 6-33 Choice of wavelengths for anomalous data collection. The peak data set (1) contains maximal anomalous Bijvoet differences. Dispersive differences between data sets are maximal for low-energy remote and high-energy remote data sets against the inflection data set (2). High-energy remote data (3) carry, in addition to the dispersive signal against inflection data, internal anomalous differences; the low remote data (4) produce only dispersive differences against inflection data. Remote data sets are usually recorded a few hundred eV below or above the absorption edge.